J. Electrochem. Sci. Eng. **12(5)** (2022) 975-987; http://dx.doi.org/10.5599/jese.1405

Open Access : : ISSN 1847-9286
www.jESE-online.org

Original scientific paper

Experimental and theoretical investigations of new Schiff base compound adsorption on aluminium in 1 M HCl

Hojat Jafari[1,✉], Elham Ameri[1,✉], Fariba Soltanolkottabi[1], Avni Berisha[2] and Mahamadou Seydou[3]

[1]*Department of Chemical Engineering, Shahreza Branch, Islamic Azad University, P.O. Box 311-86145 Shahreza, Iran*

[2]*Department of Chemistry, Faculty of Natural and Mathematics Science, University of Prishtina, 10000 Prishtina, Kosovo*

[3]*Université de Paris, CNRS, ITODYS UMR 7086, 15 rue J.A. de Baïf, F-75013 Paris, France*

Corresponding authors: ✉ hojatjafari80@yahoo.com, ✉ ameri@iaush.ac.ir

Received: June 13, 2022; Accepted: July 7, 2022; Published: August 11, 2022

Abstract

The new Schiff base, 2,2'-((1Z,1'Z)-(((propane-1,3-diylbis(oxy))bis(2,1-phenylene))bis(methanylylidene))bis(azanylylidene))diethanol, was investigated as a corrosion inhibitor of aluminium in 1 M HCl. Polarization and electrochemical impedance measurements were used for this purpose. Polarization curves showed that the compound is a mixed-type corrosion inhibitor. Also, the results showed an increase in inhibition efficiency as the concentration of the compound increased. The maximum corrosion inhibition efficiency of approximately 81 % was reached at the concentration of 2 mg/L of the inhibitor. The results of the density functional theory method were consistent with the experimental results. The surface morphology of the samples was examined under atomic force microscopy.

Keywords

Acid corrosion; potentiodynamic polarization; atomic force microscopy; density functional theory.

Introduction

Corrosion of aluminium is a common process [1]. Aluminium is an active metal, but its corrosion resistance is high in most situations due to the production of aluminium oxide layer on its surface [2,3]. This oxide forms a protective layer resistant to most acidic and neutral solutions but highly vulnerable in HCl conditions [4]. As a result, numerous treatments and investigations are required to mitigate aluminium corrosion to some level [5]. To address this issue, an efficient and practical approach to avoiding metal corrosion has usually been employed, *i.e.*, the use of inhibitors [6,7]. Corrosion inhibitors are chemical compounds that, when introduced to a corrosive medium at low quantities, decrease or prevent metal corrosion [8-10]. Research on corrosion inhibition has been ongoing for years [10-14]. One of the most popular strategies for changing the active corrosion

process to inactivity is to add an organic inhibitor [15]. In industries, adding inhibitors is particularly prevalent since it can be done without pausing or affecting the process. Researchers are currently looking for a safe inhibitor that has the best effect on corrosion prevention [5-7]. The success of such large-scale inhibitor applications is dependent on slowing down the corrosion process. At present, several organic chemicals are commonly utilized in industry to reduce corrosion and manage alkaline and acidic environmental conditions [16-21]. Up to now, many organic compounds have been used to prevent aluminium corrosion in acidic solutions [1,3-5].

Schiff bases are corrosion inhibitors due to the presence of the C = N group, an electron cloud on the aromatic ring, and electronegative N, O, and S atoms in the molecule [22,23]. In the present paper, corrosion inhibition of a new Schiff base on aluminium was investigated in 1M HCl. Using polarization method and atomic force microscopy, the corrosion protection effectiveness of a Schiff base named 2,2'-((1Z,1'Z)-(((propane-1,3-diylbis(oxy))bis(2,1-phenylene))bis(methanylylidene)) bis(azanylylidene))diethanol (PPMD) for aluminium in 1M HCl was evaluated. In addition, DFT calculations were employed in conjunction with other quantum chemical methods in order to find consistency with the PPMD inhibitory performance.

Experimental

Aluminium samples cut out to squared specimens with an area of 1 cm^2 were cooled in cold epoxy resin before being polished with emery paper grades ranging from 220 to 2000 and washed with distilled water and acetone. Then, the samples were dried with air and stored in a desiccator until used for polarization tests and surface analysis. Chemical composition of Al in wt.% was: Al (99.38 %), Fe (0.25 %), Cu (0.04 %), Ti (0.06 %), Mn (0.06 %), Si (0.14 %), Mg (0.03 %) and Zn (0.04 %). For corrosion tests, a solution of 1 M HCl was prepared by diluting analytical grade 37 % HCl acid with double distilled water. Later, the inhibitor with concentrations of 0.5, 1.0, 1.5 and 2.0 mg/L was dispersed in the corrosion test solution for electrochemical studies. Ligand 2,2'-((1Z,1'Z)-(((propane-1,3-diylbis(oxy))bis(2,1-phenylene))bis(methanylylidene))bis(azanylylidene))diethanol was prepared according to literature method [24].

2-[3-(2-formyl phenoxy)propoxy] benzaldehyde (0.284 g, 1 mmol) and ethanol amine (0.122 g, 2 mmol) were mixed and heated under reflux for 3 hours in ethanol (30 ml). The solution was refined and the filtrate was reduced to cca 10 cm^3. Yield: 85 %. Anal. Calc. for $C_{21}H_{26}N_2O_4$: C, 68.09; H, 7.07; N, 17.28. Found: C, 67.74; H, 7.17; N, 17.39. IR (KBr, cm^{-1}): 1638 (υ C=N Schiff base), 1490 (νC=C), 3365 (νOH). ^{1}H NMR (DMSO, ppm, 300 MHz): δ 2.36 (m, 2H), 3.71 (t, 4H), 3.82 (t, 4H), 4.25 (t, 4H), 6.99 (m, 2H), 7.40 (m, 2H) 7.96 (m, 2H), 7.99 (m, 2 H), 875 (s, 2H). 13C NMR (DMSO, ppm, 300 MHz): δ 62.48, 63.57, 65.03, 76.73, 77.05, 112.20, 121,09, 125.62,125,74, 12684, 127.40, 132.16 (aromatic rings), 158.88 (Schiff base).

The chemical structure of the prepared Schiff base is shown in Figure 1.

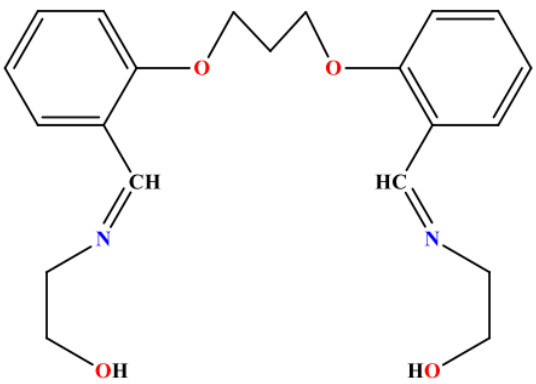

***Figure 1**. Chemical structure of Schiff base*

Autolab instrument was used to perform polarization tests. The tests were performed with a standard cell having a platinum wire as an auxiliary electrode and a saturated calomel electrode (SCE) as a reference electrode. The experiments were performed at room temperature. At the beginning of each experiment, an interval of about 30 minutes was applied to stabilize the potential of the electrode. The measurements were performed within a potential range of about -900 to -300 mV compared to the open circuit potential, with a scan rate of 1 mV/s.

Electrochemical impedance tests were performed after 30 minutes of immersion in the solutions. For this purpose, a three-electrode electrochemical cell, including counter electrode (graphite), reference electrode (SCE) and the working electrode (Al), is connected to a computer-controlled AutoLab potentiostat/galvanostat system (PGSTAT 302) and tested at the open circuit potential in the frequency range of 100 kHz to 10 mHz, and *ac* peak amplitude of 10 mV.

Atomic forced microscopy was used to study the morphology of sample surfaces. In this method, Al samples were immersed for 24 hours in 1 M HCl solution without inhibitor and also in a solution containing 2 mg/L of inhibitor at room temperature. The samples were then removed from the solution and washed with distilled water and acetone and scanned by atomic force microscopy (AFM) NanoSurf easyscan2.

To optimize adsorption of the corrosion inhibitor on metal surface atoms and prove that they are effective, it is crucial to properly examine their electronic and molecular properties. It is crucial to focus on the frontier molecular orbital as a result (FMOs). The inhibitor should affect the metal surface, in theory. In this respect, theoretical knowledge is essential to estimate the geometrical structure of adsorption and other corrosive species on the surface of metal atoms. The outcomes of this investigation, which combins molecular dynamics with Monte Carlo simulation, will be covered in depth in the following section.

FMOs were investigated using the Materials Studio program DMol^3 module. The geometrical properties of all inhibitors were optimized using the M06-L [25-28] functional in combination with a double numerical basis set and polarization to comprehend better electronic interaction and correlation (DNP) [28]. The self-consistent field converged at an energy change of less than 10^{-7} au. The conductor-like screening model (COSMO) [29-31] was employed in this study to account for the solvent-water effect.

Furthermore, potential interactions between the inhibitor molecule and Al surface atoms were examined using a Monte Carlo (MC) approach with the Adsorption locator module in Material Studio software (Materials Studio package, BIOVIA, Dassault Systèmes, San Diego, USA, 2017). A cell with dimensions of 2.8634×2.8634×2.3370 nm and a vacuum slab 4.0 nm further than Al (111) surface. The MC simulations were carried out by continuously loading the inhibitor molecules into a modelled cell with corrosive species such as 750 H_2O, 10 H_3O^+, and 10 Cl^- using the Adsorption locator module in Material Studio. Specifically, the top layer of the Al (111) slab was chosen as the target atoms during the MC simulation because it was thought to have plausible sites for adsorption of the inhibitor molecules. After the simulation, the equilibrium adsorption configuration with the lowest energy was explored and assessed.

Molecular dynamic (MD) simulations were used to simulate inhibitor adsorption on the metal surface. The density functional theory (DFT), MC, and molecular dynamics simulations for this work were performed using Material Studio. The COMPASS forcefield in Material Studio's Forcite module was used to change the geometries of the inhibitor, water, and hydronium ion (H_3O^+) [32-37].

MD simulations were provided here to investigate the interactions between a particular inhibitor, metal surface, and aqueous hydrochloric acid. Following that, the solution slabs were optimized.

Second, nine atom layers of thickness were used to construct an Al slab with a (111) plane. This slab is referred to as Al (111). This plane surface was used for the computations due to its dense structure and low energy surface. Following its development, the simulation box was geometrically optimized in order to avoid unfavorable chemical combinations and produce an energetically minimal model for future simulations. During the optimization process, the 'smart' algorithm was used. Optimization was successful since the temperature and energy fluctuation curves remained unchanged. Our next step was to run MD simulations in Material Studio's Forcite module at 295 K using the COMPASS forcefield on the optimized simulation box with all Al (111) atoms frozen but the two top layers (with a time step of 1.0 fs). The simulation was run for 1.5 ns [34,35]. Using the trajectory of the MD simulation, the radial distribution function (RDF) was generated in order to predict how the inhibitor molecule adsorbs.

Results and discussion

Polarization diagram

Figure 2 shows the polarization diagram of aluminum in 1M HCl without the presence of inhibitor and with different concentrations (0.5 – 2 mg/L) of inhibitor.

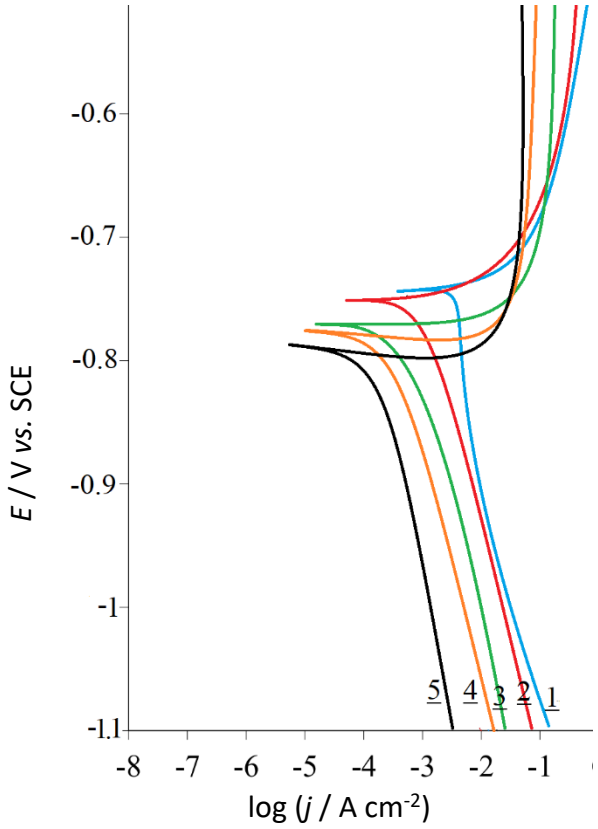

***Figure 2**. Tafel plots of Al in 1.0M HCl without and with corrosion inhibitor: blank (1); 0.5 (2); 1.0 (3); 1.5 (4); 2.0 (5) mg/L*

Electrochemical parameters, including corrosion potential (E_{corr}), corrosion current density (j_{corr}) and anodic and cathodic Tafel slopes (β_a, β_c) are estimated from Figure 2, and shown in Table 2. The degree of surface coverage (θ) and inhibitory efficiency (*IE* / %) are calculated by the following equations [12,13]:

$$\theta = \frac{j^0_{corr} - j_{corr}}{j^0_{corr}} \quad (1)$$

$$IE = \frac{j^0_{corr} - j_{corr}}{j^0_{corr}} 100 \quad (2)$$

where j^0_{corr} and j_{corr} are corrosion current densities in solution without inhibitor and in the presence of inhibitor, respectively. As shown in Table 1, the corrosion current density decreases with increasing inhibitor concentration.

Table 1. *Results derived from Tafel plots in Fig. 2*

Concentration, mg/L	$-E_{corr}$ / mV	j_{corr} / mA cm^{-2}	β_a (±1) / mV dec^{-1}	$-\beta_c$ (±1) / mV dec^{-1}	θ (±10^{-2})	*IE* / %
0.0	729	28.1	221	223	----	-------
0.5	732	17.8	203	219	0.37	37
1.0	756	12.7	197	281	0.55	55
1.5	767	8.4	195	211	0.70	70
2.0	773	5.3	194	238	0.81	81

Also, with increasing Schiff base concentration, both Tafel anode and cathode slopes didn't show any specific trend. This confirms that the inhibitor prevents corrosion by covering the active points on the metal surface [22]. The value of corrosion potential in the presence of inhibitor is reduced compared to the solution without Schiff base and with increasing concentration of the inhibitor. On the other hand, the corrosion potential is shifted to higher negative values when the inhibitor concentration rises (Figure 2), indicating a certain inhibitor impact on the cathodic branch of the polarization curve. Table 1 shows that the effectiveness of the inhibition is improved with increasing ligand concentration. Due to its clear impact on both the cathodic reaction (hydrogen and oxygen reductions) and the anodic reaction (metal dissolution), the inhibitor was of the mixed type, although the cathodic reaction is more clearly affected. In other words, the anodic dissolution energy gain is less than the hydrogen reduction energy increase. In addition, the corrosion potential changes slightly with increasing concentration, indicating a mixed mechanism of corrosion inhibition [19-21].

EIS test

Figure 3 shows the Nyquist diagrams of the aluminium electrode in HCl solution without inhibitor and with different concentrations of inhibitor.

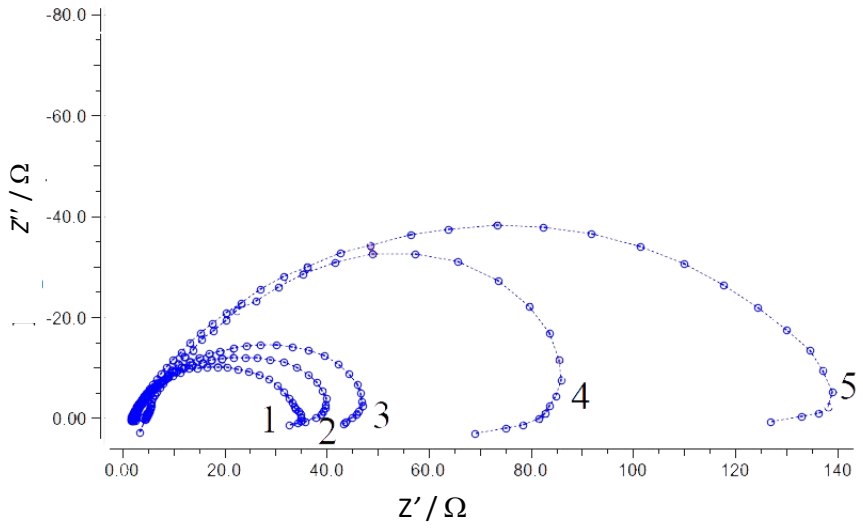

Figure 3. *Nyquist plots of Al in 1.0 M HCl in the absence and presence of the corrosion inhibitor: blank solution (1) and 0.5 (2), 1.0 (3); 1.5 (4); 2.0 (5) mg/L*

In agreement with already reported impedance spectra of aluminium AA2219-T6 alloy in HCl solution with and without ferrocenyl Schiff bases [5], impedance spectra in Figure 3 show semicircle responses at higher to medium frequencies and inductive responses at lower frequencies. As shown in Figure 3, the radius of the semicircle increases significantly with the increasing concentration of the inhibitor.

It has already been established that the appearance of a semicircle in impedance spectra of aluminium corrosion in acid media is primarily connected with double layer capacitance (C_{dl}) and charge transfer resistance (R_{ct}) at the aluminium/corrosive electrolyte interface [4,5]. A significant increase of circle diameters in Figure 3 suggests that with increasing inhibitor concentration, charge transfer resistance (R_{ct}) increases, meaning that the degree of corrosion of the aluminium in solution decreases. As the Schiff base concentration increases, the double-layer capacitance (C_{dl}) value decreases. This indicates that inhibitory molecules replace water molecules on the metal surface. The decrease in C_{dl} values caused by adsorption of inhibitor indicates that the exposed surface area decreased. On the other hand, a decrease in C_{dl}, can result from a decrease in local dielectric constant and/or increase in the thickness of the electrical double layer, which suggests that Schiff base inhibitors act by adsorption at the metal-solution interface.

Surface morphology study

The morphology of the surface of Al samples in 1 M HCl solution was examined by AFM in the presence of 2 mg/L Schiff base and without Schiff base at 25 °C and after 24 hours of immersion. The results are shown in Figure 4.

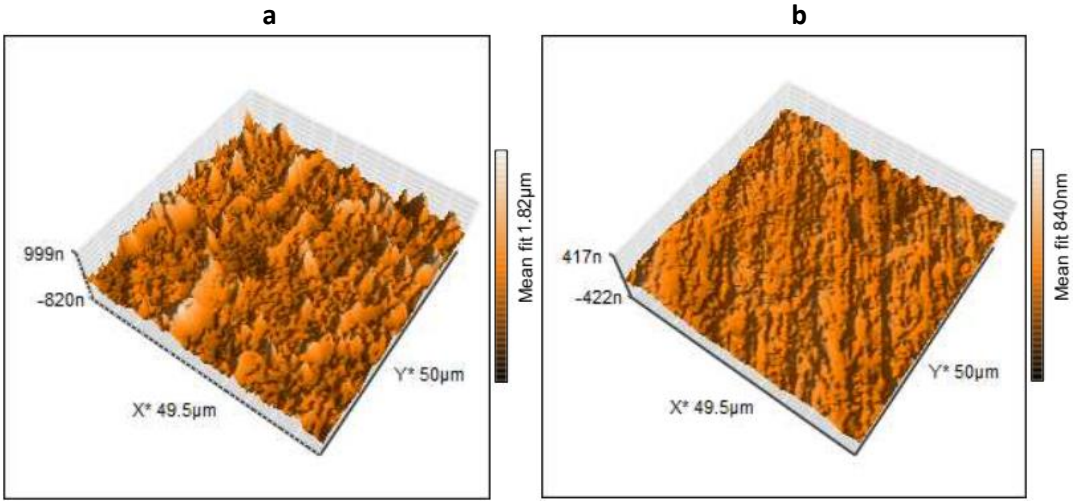

Figure 4*. AFM of aluminium electrode after 24 h of immersion in 1 M HCl solution: (a) without inhibitor; (b) with 2mg/L of inhibitor*

In the absence of an inhibitor, a rough surface is observed due to rapid corrosion by 1 M HCl. Corrosion, in this case, is relatively uniform and there is no sign of local corrosion. In the presence of the inhibitor, the aluminium surface roughness is reduced, which indicates the formation of a film on the metal surface.

DFT analysis

A conformer search (Boltzmann jump technique; the number of conformers: 8000; utilizing the COMPASS II forcefield) was undertaken in the early phase of the procedure in order to acquire the lowest feasible starting energy for the molecule while speeding up DFT computations [29-42]. Calculations for DFT were started with the lowest-energy conformer shown by the image in Figure 5.

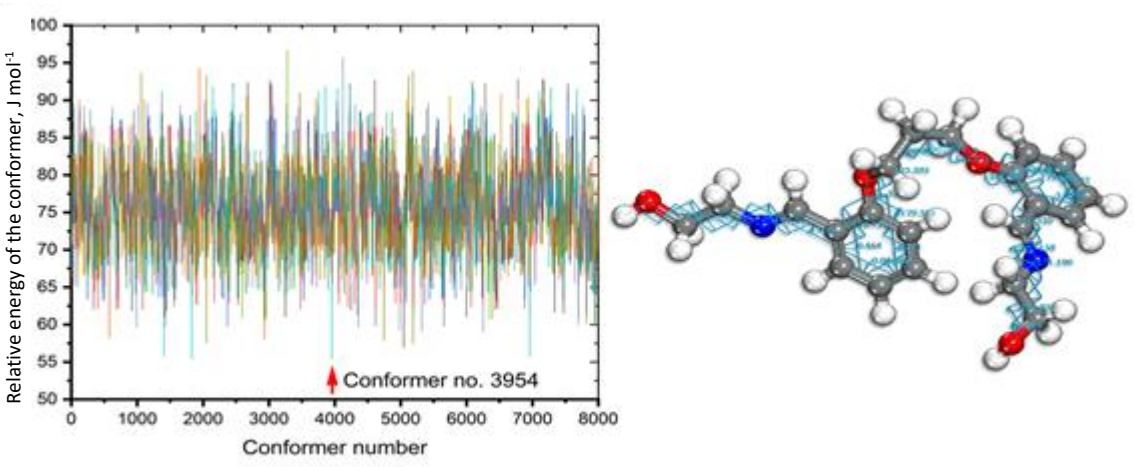

***Figure 5**. Energies of the conformer search and the resultant structure of the inhibitor*

The σ-profile (Figure 6) reveals the charge density distribution on the molecule's surface and may be used to evaluate the solubility of the conjugate in various solvents (in our case, water) [29,43].

The sigma-profile charge density curve is generated using COSMO model simulations. Partially charged atomic nuclei are utilized in COSMO to illustrate the electrostatic potential [44]. Figure 6 indicates that the inhibitor is both acceptor and donor of H-bonds. Since water molecules establish H-bond acceptor/donor connections when an inhibitor is dissolved, its solubility is regulated by this capacity.

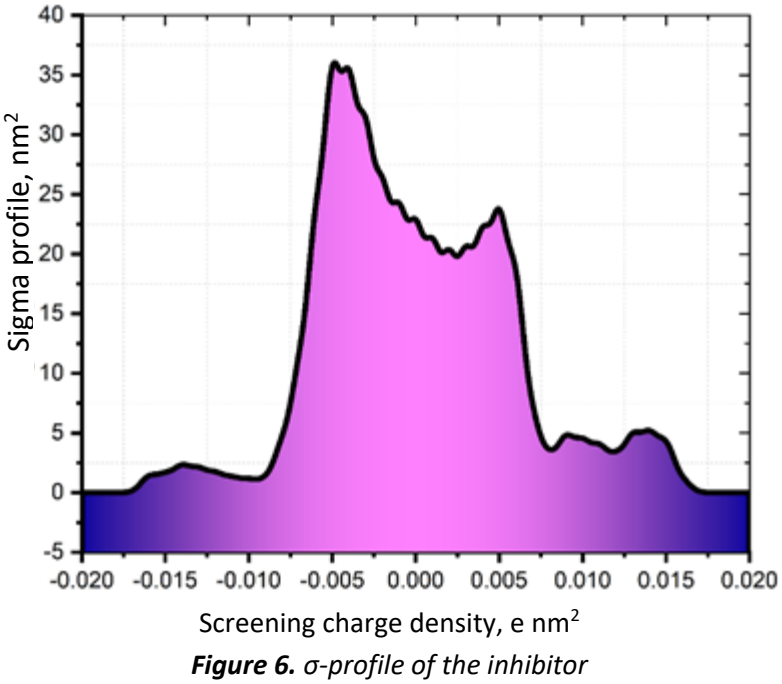

***Figure 6.** σ-profile of the inhibitor*

O and N heteroatoms, which are near the inhibitor-HOMO electron density, are also near the LUMO electron density, which is represented in Figure 7. HOMO electron density is diffused towards the molecule heteroatoms (O and N), meaning that these molecules can transmit electrons to the Al surface, as can be noticed in Figure 7. Coating a protective organic layer on metal surfaces arises from this electron sharing, which shields the metal from corrosion [41]. Electron acceptors termed LUMOs are connected to parts of the inhibitor that receive electrons from an electron surface rich in metals, such as that found in Al [44].

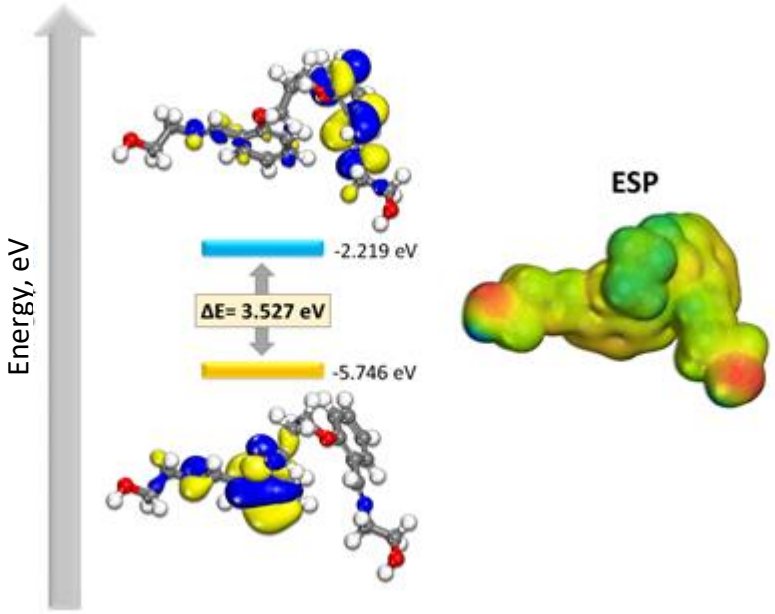

***Figure 7**. HOMO, LUMO and ESP surface of the inhibitor*

Adsorption on the metal-surface is expected to be considerably increased due to the interchange of lone pair electrons between heteroatoms (N and O) and the vacant Al d-orbital, which results in a minor boost in surface absorption potential [43].

Table 2 lists the most often reported descriptors (the formulae used to construct them may be found elsewhere [41]). A better understanding of the adsorptive behavior of inhibitors may be achieved by analyzing the DFT simulations of inhibitor adsorptive reactivity [41]. Due to their low electron affinity and high ionization potential, it is commonly thought that the adsorption of inhibitors onto the Al(111) surface is supported by its capacity to exchange electrons with the Al surface (Table 2) [41]. Chemical softness and hardness are predicted values representing the inhibitor adsorption affinity for the metal surface, as are high values of chemical softness. Inhibitors reflect the capacity to accept electrons from the Al surface [40].

***Table 2**. Calculated theoretical chemical parameters for the inhibitor*

Descriptor	Inhibitor
HOMO, eV	-5.7460
LUMO, eV	-2.2190
Δ*E*(HOMO-LUMO) / eV	3.527
Ionization energy (*I* / eV)	5.7460
Electron affinity (*A* / eV)	2.2190
Electronegativity (*X* / eV)	3.9825
Global hardness (*η* /eV)	1.7635
Chemical potential (π / J kg^{-1})	-3.9825
Global softness (σ /eV)	0.5671
Global electrophilicity (ω /eV)	4.4968
Electrodonating (ω-) power, eV	6.7085
Electroaccepting (ω+) power, eV	2.7260
Net electrophilicity (Δω+-), eV	2.5769
Fraction of transferred electrons (Δ*N* /eV)	0.0787
Energy from inhb to metal (Δ*N*/eV)	0.0109
Δ*E* back-donation / eV	-0.4409

Mulliken atomic charges (MAC) are a reliable and persuasive indication of the inhibitory sites (atoms) involved in metal adsorption. There are numerous possibilities for a description of the reaction between atoms on the Al surface with the inhibitor molecules [42].

Figure 8 illustrates the inhibitor-MAC values. The inhibitor O and N atoms have strong negative charges, indicating that these centers have the maximum density of electrons and are consequently the most effective in attaching to metal surfaces. Figure 8 displays the molecular electrostatic potential (MEP) of the inhibitors in different concentrations (the region in red).

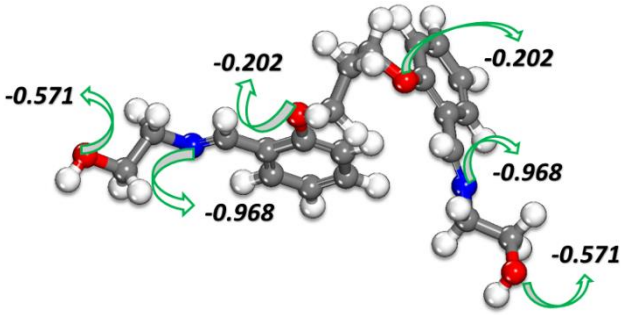

***Figure 8**. Optimized structures of the inhibitor and their Mulliken atomic charges (MAC)*

MC and MD simulations

Using the Al(111) surface as a starting point, the adsorption energetics of the system may be calculated readily. It is feasible to compute the adsorption energy (E_{ads}) by using the following equation (3) [42]:

$$E_{adsorption} = E_{Al(111)||inhibitor} - (E_{Al(111)} + E_{inhibitor}) \quad (3)$$

where $E_{Al(111)||inhibitor}$ is the total energy of the simulated system, $E_{Al(111)}$ and $E_{inhibitor}$ is the total energy of the Al(111) surface and the corresponding free inhibitor molecules.

After MC calculations were completed successfully, a comprehensive investigation of the inhibitor-adsorption geometry was done to validate the findings. The MC simulation capacity to establish equilibrium may be validated using the steady-state energy levels. The system-minimal energy state was obtained roughly halfway through the experiment. As demonstrated in Figure 9, the real arrangement of the adsorbent inhibitors is represented on a simulated Al (111) plane.

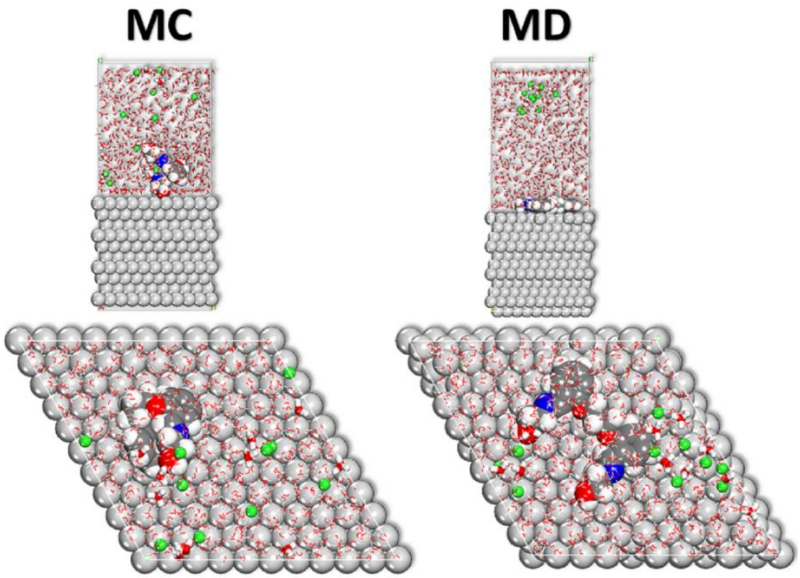

***Figure 9**. MC and MD possess the lowest adsorption configurations for inhibitor adsorption in the simulated corrosion media on the Al substrate*

Al (111) surface is being decorated by the inhibitor in virtually (in the case of MD) a parallel direction to the inhibitor. We suggest that this adsorption pattern on the Al (111) plane may be induced by an inhibitor molecule's backbone binding the plane's surface atoms (overseen by heteroatoms). The molecules' inclination to expose their heteroatoms and electron rings to the surface leads to adsorption, which provides the molecules with their adsorptive abilities [42].

Inhibitor's adsorption reflects a relatively large E_{ads} (Figure 10) on the metal surface. Because of the extraordinarily high adsorption energies, the inhibitor has a strong adsorption interaction with the metal. Using this contact, the metal surface is protected from corrosion by the development of a protective layer [41].

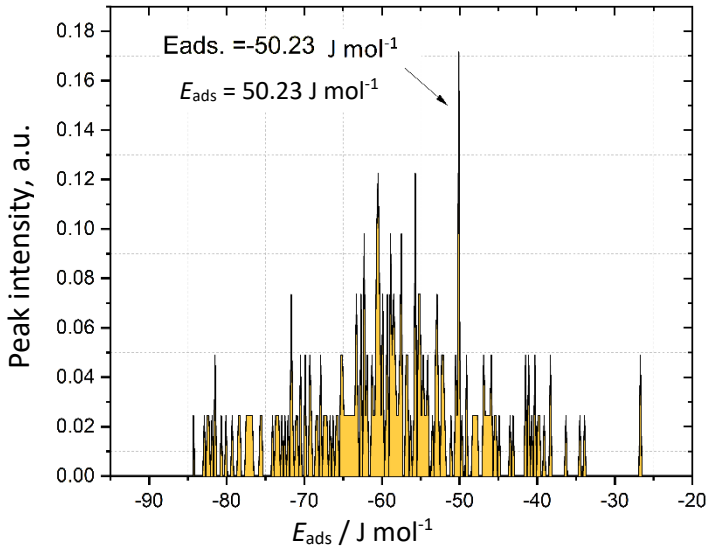

***Figure 10**. Distribution of adsorption energies of the inhibitor obtained from MC calculations*

MD is extensively considered a correct representation of the adsorption dynamics [32,33,35,39]. It is evident that after several hundreds of ps of NVT simulation, the inhibitors (Figure 9) adopt a somewhat flat structure on one side of the molecule rings onto the metal surface and is strongly adsorbed onto the Al surface. As demonstrated in Figure 11, the adsorption energy is rather high, with a minor decline in energy as temperature increases, which is consistent with the experimental findings.

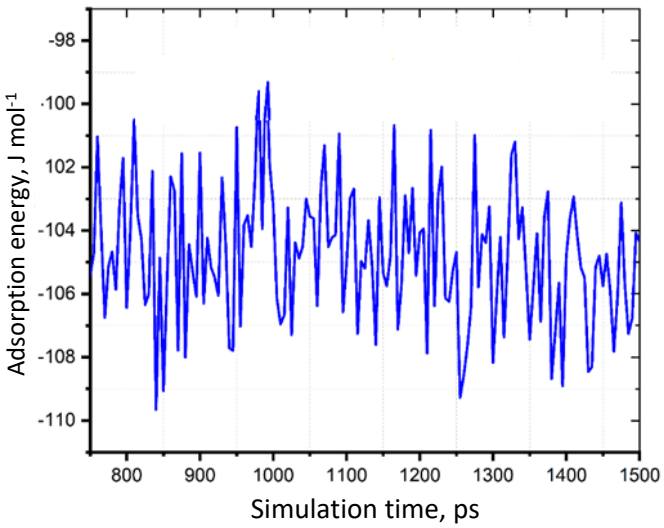

***Figure 11.** Interaction energy of the inhibitor at the Al surface during the second half of MD*

Corrosion inhibitor adsorption on metal surfaces may be explored utilizing the RDF analysis of the MD trajectory obtained during corrosion simulations, which is a basic and uncomplicated way [42].

Adsorption processes on metal surfaces may be determined from the RDF graph if peaks occur at a given distance from the metal surface [42]. Heights are believed to reflect chemisorbable processes when detected in the region of 0.1–0.35 nm in length; nevertheless, for physical adsorption, RDF peaks are expected to be present at distances larger than 0.35 nm. Al surface and inhibitor heteroatoms (N and O) showed RDF peak values at distances of less than 0.35 nm (Figure 12) [42]. In this scenario, the inhibitor appears to be strongly interacting with the metal surface, as suggested by its comparatively high negative adsorption energy (as obtained for MC and MD) value and RDF peaks.

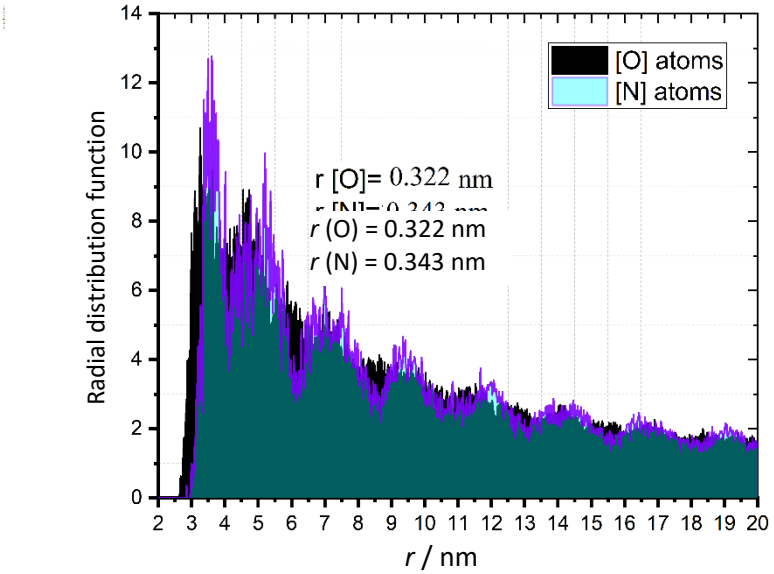

***Figure 12**. RDF of heteroatoms (O and N) for the inhibitor on Al surface accomplished from MD trajectory analysis*

Conclusion

In this study, the effects of corrosion inhibition and the ability of adsorption of a new Schiff base (PPMD) on the Al surface were investigated and the following results were obtained: The organic compound PPMD has inhibition properties in 1 M HCl medium. AFM analysis supports the creation of a preventive layer of inhibitor on Al surface, which facilitates the lowering of corrosion rate. This inhibitor affects both anodic and cathodic branches and reduces the corrosion rate by blocking existing sites by reducing the exchange current of reactions. It has been demonstrated by the MD calculations that inhibitors are relatively flat-adsorbed only on one side of the molecule, resulting in the exposure of their adsorption centers to the surface of aluminium. The adsorption energies that have been obtained are relatively high and compatible with experimental findings. This implies that a large quantity of inhibitor adsorption takes place on the metal, resulting in greater corrosion protection.

References

[1] C. S. Proença, B. Serrano, J. Correia, M. E. M. Araújo, *Metals* **12(3)** (2022) 508. https://doi.org/10.3390/met12030508

[2] J. Ryl, I. Wysocka, M. Cieslik, H. Gerengi, T. Ossowski, S. Krakowiak, P. Niedzialkowski. *Electrochimica Acta* **304** (2019) 263-274. https://doi.org/10.1016/j.electacta.2019.03.012

[3] S. Bashir, H. Lgaz, I. M. Chung, A. Kumar, *Chemical Engineering Communications* **3(8)** (2021) 1121-1130. https://doi.org/10.1080/00986445.2020.1752680

[4] S. Chaudhary, R. K. Tak, *Biointerface Research in Applied Chemistry* **12** (2022) 2603-2617. https://doi.org/10.33263/BRIAC122.26032617
[5] U. Nazir, Z. Akhter, N. K. Janjua, M. A. Asghar, S. Kanwal, T. M. Butt, A. Sani, F. Liaqat, R. Hussain, F. U. Shah, *RSC Advances* **10(13)** (2020) 7585-7599. https://doi.org/10.1039/C9RA10692H
[6] D. Kumari, P. P. Venugopal, D. Chakraborty, *Journal of Adhesion Science and Technology* **10** (2021). https://doi.org/10.1080/01694243.2021.1999703
[7] S. C. Udensi, O. E. Ekpe, L. A. Nnanna, *Chemistry Africa* **3(2)** (2020) 303-316. https://doi.org/10.1007/s42250-020-00131-w
[8] H. Jafari, K. Akbarzade, I. Danaee, *Arabian Journal of Chemistry* **12(7)** (2019) 1387-1394. https://doi.org/10.1016/j.arabjc.2014.11.018
[9] K. Sayin, N. Kurtoglu, M. Kose, D. Karakas, M. Kurtoglu, *Journal of Molecular Structure* **1119** (2016) 413-422. https://doi.org/10.1016/j.molstruc.2016.04.097
[10] K. Sayin, D. Karakaş, N. Karakuş, T. Alagöz Sayin, Z. Zaim, S. Erkan Kariper, *Polyhedron* **90** (2015) 139-146. https://doi.org/10.1016/j.poly.2015.01.047
[11] L. L. Liao, S. Mo, H. Q. Luo, N. B. Li, *Journal of Colloid and Interface Science* **520** (2018) 41-49. https://doi.org/10.1016/j.jcis.2018.02.071
[12] H. Jafari, K. Sayin, *Journal of the Taiwan Institute of Chemical Engineers* **64** (2016) 314-24. https://doi.org/10.1016/j.jtice.2016.04.021
[13] H. Jafari, K. Sayin, *Journal of the Taiwan Institute of Chemical Engineers* **56** (2015) 181-90. https://doi.org/10.1016/j.jtice.2015.03.030
[14] H. Jafari, Z. Jafari, *Journal of Bio- and Tribo-Corrosion* **4** (2018) 24. https://doi.org/10.1007/s40735-018-0139-y
[15] M. N. Desai, M. B. Desai, C. B. Shah, S. M. Desai, *Corrosion Science* **26(10)** (1986) 827-837. https://doi.org/10.1016/0010-938X(86)90066-1
[16] H. Yang, M. Zhang, A. Singh, *International Journal of Electrochemical Science* **13** (2018) 9131-9144. https://doi.org/10.20964/2018.09.62
[17] H. Jafari, I. Danaee, H. Eskandari, M. RashvandAvei, *Journal of Materials Science & Technology* **30(3)** (2014) 239-252. https://doi.org/10.1016/j.jmst.2014.01.003
[18] H. Jafari, I. Danaee, H. Eskandari, M. RashvandAvei, *Industrial & Engineering Chemistry Research* **52** (2013) 6617-6632. https://doi.org/10.1021/ie400066x
[19] A. S. Fouda, A. M. El-Desoky, H. M. Hassan, *International Journal of Electrochemical Science* **8** (2013) 5866-5885.
[20] M. A. Quraishi, D. Jamal, M. Luqman, *Indian Journal of Chemical Technology* **9** (2002) 479-483.
[21] O. O. Fadare, A. E. Okoronkwo, E. F. Olasehinde, *African Journal of Pure and Applied Chemistry* **10(1)** (2016) 8-22. https://doi.org/10.5897/AJPAC2015.0651
[22] S. S. Al-Najjar, A. Y. Al-Baitai, *Physical Chemistry Research* **10(2)** (2022) 179 194. https://www.physchemres.org/article_139374_e9ace04e1b61b5c8f0c0e93cb540f3b5.pdf
[23] H. M. Abd El-Lateef, K. A. Soliman, M. A. Al-Omair, M. S. S. Adam, *Journal of the Taiwan Institute of Chemical Engineers* **120** (2021) 391-408. https://doi.org/10.1016/j.jtice.2021.03.036
[24] M. Rezaeivala, S. Karimi, B. Tuzun, K. Sayin, *Thin Solid Films* **741** (2022) 139036. https://doi.org/10.1016/j.tsf.2021.139036
[25] Y. Zhao, D. G. Truhlar, *Theoretical Chemistry Accounts* **120** (2008) 215-241. https://doi.org/10.1007/s00214-007-0310-x
[26] M. Ben Hadj Ayed, T. Osmani, N. Issaoui, A. Berisha, B. Oujia, H. Ghalla, *Theoretical Chemistry Accounts* **138** (2019) 84. https://doi.org/10.1007/s00214-019-2476-4

[27] N. Mardirossian, M. Head-Gordon, *Molecular Physics* **115(19)** (2017) 2315-2372. https://doi.org/10.1080/00268976.2017.1333644
[28] Y. Inada, H. Orita, *Journal of Computational Chemistry* **29(2)** (2008) 225-232. https://doi.org/10.1002/jcc.20782
[29] A. Klamt, *COSMO-RS: From quantum chemistry to fluid phase thermodynamics and drug design*, Elsevier, 2005.
[30] A. Klamt, *Wiley Interdisciplinary Reviews: Computational Molecular Science* **8** (2018) e1338. https://doi.org/10.1002/wcms.1338
[31] A. Berisha, *Journal of Chemistry* **2019** (2019) 5126071. https://doi.org/10.1155/2019/5126071
[32] O. Dagdag, A. El Harfi, L. El Gana, Z. S. Safi, L. Guo, A. Berisha, C. Verma, E. E . Ebenso, N. Wazzan, M. El Gouri, *Journal of Applied Polymer Science* **138(2)** (2021) 49673. https://doi.org/10.1002/APP.49673
[33] M. El Faydy, H. About, I. Warad, Y. Kerroum, A. Berisha, F. Podvorica, F. Bentiss, G. Kaichouh, B. Lakhrissi, A. Zarrouk, *Journal of Molecular Liquids* **342** (2021) 117333. https://doi.org/10.1016/J.MOLLIQ.2021.117333
[34] A. Molhi, R. Hsissou, M. Damej, A. Berisha, V. Thaçi, A. Belafhaili, M. Benmessaoud, N. Labjar, S. El Hajjaji, *International Journal of Corrosion and Scale Inhibition* **10(1)** (2021) 399-418. https://doi.org/10.17675/2305-6894-2021-10-1-23
[35] M. Alahiane, R. Oukhrib, A. Berisha, Y. A. Albrimi, R. A. Akbour, H. A. Oualid, H. Bourzi, A. Assabbane, A. Nahlé, M. Hamdani, *Journal of Molecular Liquids* **328** (2021) 115413. https://doi.org/10.1016/J.MOLLIQ.2021.115413
[36] P. K. Uppalapati, A. Berisha, K. Velmurugan, R. Nandhakumar, A. Khosla, T. Liang, *International Journal of Quantum Chemistry* **121(9)** (2021) e26600. https://doi.org/10.1002/QUA.26600
[37] R. Haldhar, D. Prasad, I. Bahadur, O. Dagdag, A. Berisha, *Journal of Molecular Liquids* **323** (2021) 114958. https://doi.org/10.1016/J.MOLLIQ.2020.114958
[38] O. Dagdag, A. Berisha, V. Mehmeti, R. Haldhar, E. Berdimurodov, O. Hamed, S. Jodeh, H. Lgaz, E.-S. M. Sherif, E. E. Ebenso, *Journal of Molecular Liquids* **346** (2021) 117886. https://doi.org/10.1016/J.MOLLIQ.2021.117886
[39] A. Ouass, M. Galai, M. Ouakki, E. Ech-Chihbi, L. Kadiri, R. Hsissou, Y. Essaadaoui, A. Berisha, M. Cherkaoui, A. Lebkiri, E. H. Rifi, *Journal of Applied Electrochemistry* **51** (2021) 1009-1032. https://doi.org/10.1007/S10800-021-01556-Y
[40] M. Damej, R. Hsissou, A. Berisha, K. Azgaou, M. Sadiku, M. Benmessaoud, N. Labjar, S. El hajjaji, *Journal of Molecular Structure* **1254** (2022) 132425. https://doi.org/10.1016/J.MOLSTRUC.2022.132425
[41] H. Jafari, M. Rezaeivala, N. Mokhtarian, A. Berisha, E. Ameri, *Journal of Bio- and Tribo-Corrosion* **8** (2022) 81. https://doi.org/10.1007/s40735-022-00679-9
[42] L. J. Yu, J. Zhang, G. M. Qiao, Y. G. Yan, Y. Ti, Y. Zhang, *Materials and Corrosion* **64(3)** (2013) 225-230. https://doi.org/10.1002/maco.201106141
[43] A. Jarray, V. Gerbaud, M. Hemati, *Progress in Organic Coatings* **101** (2016) 195-206. https://doi.org/10.1016/j.porgcoat.2016.08.008
[44] A. Berisha, *Journal of Chemistry* **2019** (2019) 5126071. https://doi.org/10.1155/2019/5126071